This article is a post-print copy of R. Ding, Y. Xia, T. Mauldin, M. R. Kessler: Biorenewable ROMP-based Thermosetting Copolymers from Functionalized Castor Oil Derivative with Various Cross-linking Agents, *Polymer*, 2014, 55(22), 5718-5726. doi:10.1016/j.polymer.2014.09.023.

Biorenewable ROMP-based thermosetting copolymers from functionalized castor oil derivative with various cross-linking agents

Rui Ding[a],
Ying Xia[a],
Timothy C. Mauldin[a],
Michael R. Kessler[a, b]

[a] Department of Materials Science and Engineering, Iowa State University, Ames, USA
[b] School of Mechanical and Materials Engineering, Washington State University, Pullman, USA

Abstract

A new norbornenyl-functionalized castor oil alcohol (NCA) was synthesized and ring-opening metathesis copolymerized separately with two norbornene-based cross-linking agents: dicyclopentadiene (DCPD) and a bifunctional norbornene crosslinker (CL). Isothermal differential scanning calorimetry (DSC) was used to examine the cure behavior of NCA/DCPD and NCA/CL resins, through which a reasonable cure schedule was determined. The glass transition temperature (T_g) and storage modulus (E'), characterized by dynamic mechanical analysis (DMA), increased significantly in both copolymer systems with the addition of cross-linking agents. Cross-link density of the two systems was evaluated using a modified empirical equation from the kinetic theory of rubber elasticity. Differences in tensile stress-strain behavior and thermal stability between polymerized NCA/DCPD and NCA/CL were correlated to the structural rigidity and cross-linking density resulting from the cross-linking agents.

Graphical abstract

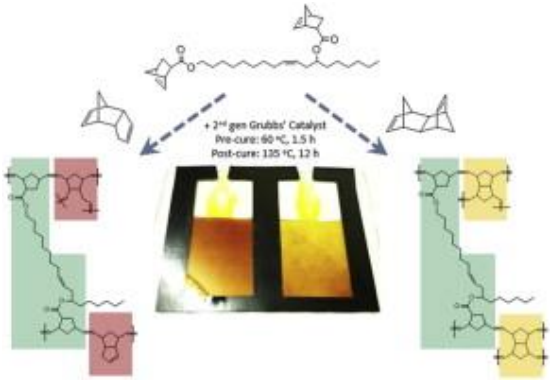

Keywords

- Castor oil;
- Norbornenyl functionality;
- Cross-linking

1. Introduction

In recent decades, increasing concerns for the environment and sustainability have prompted the exploration of bio-based, renewable plastics and composites for structural applications. Among the candidates for renewable resources, agricultural oils have emerged as a powerful feedstock to develop polymeric materials capable of replacing commercial polymer products currently derived from petrochemicals. The polymerization and processing of agricultural oils into stiff, robust materials in key applications, such as automotive components, civil engineering and construction are on-going topics in both academic and industrial settings [1].

Hardening of drying oils, such as tung oil, readily occurs due to their inherently high extent of unsaturation, but the majority of fatty acid chains of agricultural oils that possess few double bonds that are not readily polymerizable (i.e., non-conjugated). Chemical modification of double bonds and ester groups on triglycerides therefore is a powerful strategy to guide monomer design towards controllable polymerization of agricultural oils. Through conversion of olefins to more reactive functional groups, such as epoxy, hydroxyl or cyclic groups, the triglyceride is susceptible to alternate polymerization paradigms or to subsequent functionalization [2]. A remarkable range of polymers have been prepared from agricultural oils utilizing various mechanisms, including free-radical polymerization, cationic polymerization, olefin metathesis polymerization, and condensation polymerization, have been reviewed [3] and [4].

Many recent efforts have concentrated on optimization of the thermal and mechanical properties of agricultural oil-based polymers. Because of the linear, flexible hydrocarbon chains common in triglycerides, which are associated with high degree of chain rotation and multiple segment movements, the resulting polymers usually exhibit low T_g and modulus [5]. Two approaches to enhance the thermal and mechanical performance of these polymers exist. First, polymer stiffness can be improved through introduction of "rigid" chemical moieties to the polymer structure, such as aromatic, carbocyclic and heterocyclic groups [6]. Second, material properties can be tuned by varying the level of covalent cross-linking in the polymer network. To achieve this, the number of functional groups on the triglyceride molecules are commonly altered. For soybean oil-based polymers, the hydroxyl functionalities per fatty chain can be manipulated by chemical reactions such as glycerolysis, amidation, methanolysis, and ester reduction, which endow the resulting polymers more cross-linking sites and significantly improved T_g and modulus [7], [8] and [9]. The addition of bifunctional, cross-linking comonomers from petroleum-derivatives is another suitable approach, although it partly compromises the bio-based content of the materials. Divinylbenzene and norbornene-based cross-linkers have gained increased attention in optimizing thermo-mechanical properties [10], [11], [12] and [13] because they serve to both cross-link the polymer and incorporate rigidity to stiffen the bio-based polymers.

Ring-opening metathesis polymerization (ROMP) has recently proven promising for developing strong and tough thermosets derived from vegetable oils. Due to the unique characteristic of olefin retention during ROMP, the resultant polymers have the potential to serve as reactive sites in the polymer matrix for self-healing composite applications [14]. Commercial Ruthenium-based catalysts are capable of initiating polymerization of modified agricultural oil-derived monomers due to such catalyst's high reactivity, functional group tolerance, and air/moisture insensitivity. Early work in ROMP of oils was explored by copolymerizing Dilulin™ [15], a commercially available norbornenyl-modified linseed oil derivative (Cargill Inc, MN), with various crosslinkers [11] and [16]. However, the low number of norbornenyl groups (≤1 per triglyceride) in Dilulin inhibits network formation with its comonomer, resulting in a plasticization effect that decreases mechanical properties. To overcome the disadvantage of incomplete network formation, norbornenyl-modified fatty alcohols derived by reacting 5-norbornene-2,3-dicarboxylate anhydride with Dilulin and castor oil (NMDA and NMCA) were synthesized [7], resulting in an average of 1.3 and 1.9 pendent norbornene groups per fatty chain, thereby improving storage modulus and T_g without the need for comonomers. Another novel copolymer system was prepared from norbornenyl-functionalized castor oil (NCO) and castor oil alcohol (NCA), which were derived by reacting 5-norbornene-2-carbonyl chloride with castor oil and castor oil alcohol respectively [8]. NCA monomer has approximately 1.8 norbornenyl groups per fatty chain, which led to relatively short gelation time and high cross-link density. The molecular structure of the aforementioned ROMP-reactive bio-monomers based on agricultural oils are listed in Fig. 1(a–e).

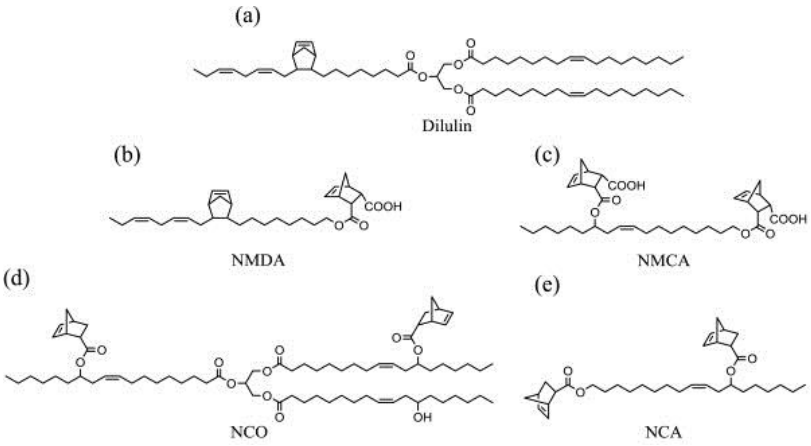

Fig. 1: ROMP-reactive bio-monomers from Dilulin and castor oil; (a) cyclopentadiene-modified linseed oil (Dilulin); (b) norbornenyl-modified Dilulin alcohol (NMDA); (c) norbornenyl-modified castor oil alcohol (NMCA); (d) norbornenyl-functionalized castor oil (NCO); and (e) norbornenyl-functionalized castor oil alcohol (NCA).

In this work, we investigate the effect of cross-linking functionality of ROMP-reactive comonomers on the thermo-mechanical properties and the network structure of the NCA thermosetting system. Two cyclic olefin comonomers, dicyclopentadiene (DCPD) and norbonene crosslinker (CL) were ring-opening metathesis copolymerized with NCA monomer in varied ratios. The cure behavior of NCA-DCPD and NCA-CL is tied to the ROMP reactivity of multifunctional cross-linking agents [11], [16] and [17]. Isothermal conversion and conversion rate of these two systems during cure were monitored using differential scanning calorimetry

(DSC). The thermo-mechanical properties of cured copolymers, polyNCA/DCPD and polyNCA/CL, were characterized using dynamic mechanical analysis (DMA). Glass transition temperature, storage modulus, loss modulus and tangent peak served as useful metrics to probe structural network changes. Mechanical properties obtained from tensile tests and thermal stability measured by thermogravimetric analysis (TGA) are also discussed.

2. Experimental

2.1. Materials

Castor oil, dicyclopentadiene (DCPD), lithium aluminum hydride (95%) (LAH), 5-norbornene-2-carboxylic acid (98%, a mixture of *endo*- and *exo*-, predominantly *endo*), thionyl chloride (99.5%) ($SOCl_2$), triethylamine (TEA) and 2nd generation Grubbs' catalyst [1,3-bis-(2,4,6-trimethylphenyl)-2-imidazolidinylidene]dichloro(phenylmethylene)(tricyclohexylphosphine) ruthenium] were obtained from Sigma–Aldrich (Milwaukee, WI). Tetrahydrofuran (HPLC grade) (THF), ethyl acetate, methylene chloride (ACS certified) (CH_2Cl_2), anhydrous magnesium sulfate ($MgSO_4$), sodium hydroxide (NaOH), sodium carbonate (Na_2CO_3), and hydrochloric acid (HCl) were supplied by Fisher Scientific (Fair Lawn, NJ). CH_2Cl_2 was refluxed over CaH_2 under nitrogen flow and distilled immediately prior to use. All other reagents were used as received without further purification.

Norbornenyl-based cross-linker (CL), a mixture of *exo-endo* isomer, 1,4,4a,5,8,8a-hexahydro-1,4,5,8-exo,-endo-dimethanonaphthalene and *endo–endo* isomer, 1,4,4a,5,8,8a-hexahydro-1,4,5,8-endo,-endo-dimethanonaphthalene in a molar ratio of 87:13, was synthesized according to a literature method [18].

2.2. Synthesis of bicyclo[2.2.1]-hept-2-ene-5-carbonyl chloride

The preparation of bicyclo[2.2.1]-hept-2-ene-5-carbonyl chloride was modified from a reported approach [19]: 5-norbornene-2-carboxylic acid (110.53 g, 0.8 mol) was mixed with thionyl chloride (190.35 g, 1.6 mol) in a 500 mL round-bottom flask, and then refluxed under dry nitrogen gas at 70 °C for 3 h. Excess $SOCl_2$ was evaporated under reduced pressure. The crude product was further purified by distillation to eliminate colored impurity, yielding a transparent liquid (71%). ^{1}H NMR (400 Hz, $CDCl_3$) indicates that the product is an mixture of *endo* isomer (74%) and *exo* isomer (26%). ^{1}H NMR δ: 6.25–6.27 (m, 1H, =CH, endo), 6.20–6.22 (m, 0.35H, =CH, exo), 6.11–6.14 (m, 0.35H, CH, exo), 6.02–6.04 (m, 1H, =CH, endo), 3.43–3.47 (m, 2H, endo), 3.29 (s, 0.35H, exo), 2.99 (s, 1.4H), 2.72–2.76 (m, 0.35H, exo), 2.00–2.05 (m, 0.36H, exo), 1.92–1.98 (m, 1.1H, endo), 1.47–1.55 (m, 2.9H), 1.41–1.43 (d, 0.36H, exo), 1.32–1.34 (d, 1.1H, endo).

2.3. Synthesis of norbornenyl-functionalized castor oil alcohol (NCA)

NCA monomer was synthesized by following the reported route [18]: LAH (12.27 g, 0.32 mol) was added to a 2000 mL, two-neck round-bottom flask with 100 mL of THF. Castor oil (100 g, 0.11 mol) was dissolved in 600 mL of THF and added dropwise to the LAH slurry in an ice bath.

The reaction was maintained at 0 °C for 12 h under mechanical stirring. To remove the remaining LAH, the reaction mixture was quenched by ice water, and then 1 M HCl was added until it changed to a clear solution. The product was extracted with ethyl acetate (600 mL), washed with water (600 mL), and then the organic layer was dried over $MgSO_4$. After solvent evaporation, the castor oil alcohol was obtained as a clear, light yellow viscous liquid (85%).

Castor oil alcohol (50 g, 0.18 mol) was dissolved in 250 mL of anhydrous CH_2Cl_2 and cooled to 0 °C in an ice bath. A solution of bicyclo[2.2.1] hept-2-ene-5-carbonyl chloride (57.8 g, 0.37 mol) in 250 mL of anhydrous CH_2Cl_2 was added dropwise and then followed by the addition of triethylamine (39.13 g, 0.39 mol). The reaction was allowed to warm to ambient temperature and the solution was stirred for 24 h. Then the reaction product was poured into 1000 mL of 5 wt.% Na_2CO_3 aqueous solution and stirred for 12 h. Product was extracted with CH_2Cl_2, dried over $MgSO_4$ and removal of solvent yielded NCA as a light brown oil (80%).

2.4. Sample preparation

Blends of NCA and cross-linking agents (DCPD or CL) were prepared at different comonomer loadings: 10, 20, 30, 50 wt.%. CL (m.p. 12 °C, determined by DSC) was mixed directly at room temperature, while DCPD (m.p. 33 °C) was melted in an oven prior to mixing with NCA. Homogenous solutions were obtained for all blend compositions.

2nd generation Grubbs' catalyst was freeze-dried prior to dissolution in monomer [20]. In a typical example, catalyst (100 mg) was dissolved in 2 mL of benzene in a small vial and then flash-frozen in a liquid nitrogen bath. The frozen solution was placed in an ice bath under vacuum for 5 h to sublime the benzene. Freeze-dried 2nd generation Grubbs' catalyst (0.125 wt.%) was added to a resin mixture cooled in an ice bath, which was vigorously stirred with a spatula for 10 s to dissolve the catalyst completely. Small amounts of resin mixture (~100 mg) was withdrawn for the cure kinetics study. The remaining resin was injected into rubber molds (100 mm × 70 mm × 1 mm) that were sandwiched between two glass plates. Specimens were cured according to the following schedule (cure schedule developed vide infra, Section 3.1): isothermal cure at 60 °C for 1.5 h, followed by post-cure at 135 °C for 12 h. After curing the resulting thermosets were removed from the oven and cooled down in the air. The ROMP of NCA/DCPD and NCA/CL mixtures is illustrated in Scheme 1.

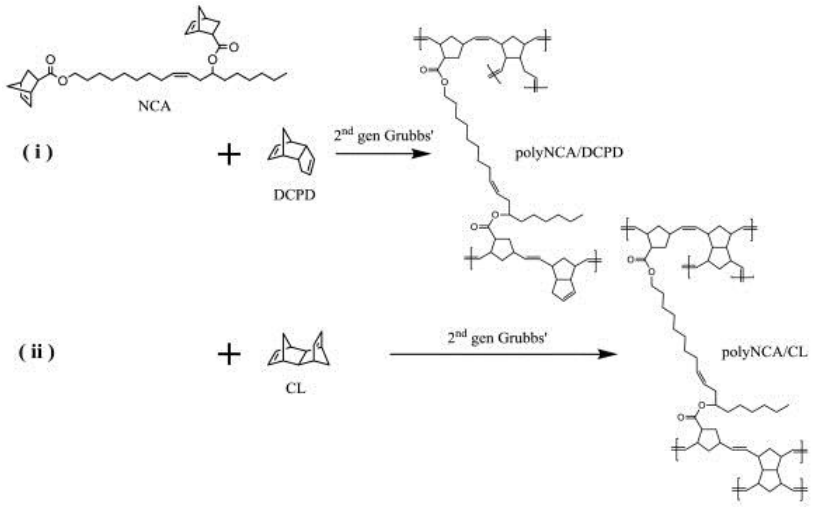

Scheme 1: ROMP of NCA with DCPD and CL.

2.5. Characterization

Differential scanning calorimetry (DSC, Q2000, TA instruments) was used to monitor isothermal curing. Resin (~10 mg) was loaded into the DSC cell at a standby temperature of −50 °C. After thermal equilibration for 1 min, the DSC cell was heated to the required temperature (T_c = 50, 60, 70 °C) at a heating rate of 100 °C/min and held isothermally for 1 h. Resulting cured samples were cooled to −50 °C at a rate of 10 °C/min, followed by a dynamic scan to 250 °C at a rate of 10 °C/min to reach full conversion.

Soxhlet extraction was performed on ca. 2.5 g samples with 100 mL of refluxing CH_2Cl_2 in a Soxhlet extractor for 24 h. After extraction both the remaining solid and the extracts were dried in a vacuum oven at 60 °C overnight.

Swelling tests of polyNCA/DCPD and polyNCA/CL were performed on small rectangular pieces (1 × 10 × 20 mm). Pre-weighed samples ($W_{initial}$) were soaked in CH_2Cl_2 for 48 h at room temperature. The final weight (W_{final}) of saturated samples was used in equation (3) to calculate swelling percentage:

$$\text{Swelling}(\%) = \frac{W_{final} - W_{initial}}{W_{initial}} \times 100\% \quad (3)$$

Dynamic mechanical analysis (DMA, Q800, TA Instruments) was performed on rectangular sample strips of 20 × 4.3 × 0.8 mm (length × width × thickness), measured in a tension fixture, with uniaxial oscillation at a constant frequency of 1 Hz and amplitude of 15 μm. The samples were scanned at a temperature range of −50 °C to 200 °C at a heating rate of 3 °C/min.

The tensile properties of the thermosetting copolymers were measured using an Instron universal testing machine (model 4502) with a crosshead speed of 50 mm/min. Testing specimens (ASTM D 638-03, type V) were machine-milled, and at least three replicates of each sample were taken

for measurement. Young's modulus (E), maximum tensile strength (σ_m), strain at break (ε_b), and tensile toughness of the polymers were recorded.

Thermal stability was investigated using a thermogravimetric analyzer (TGA) Q50 (TA Instruments). PolyNCA/DCPD and polyNCA/CL samples (~10 mg) were heated from ambient temperature to 700 °C at a heating rate of 20 °C/min in air (50 mL/min).

3. Results and discussion

3.1. Isothermal cure kinetics

Isothermal curing was performed at three temperatures 50, 60, and 70 °C for NCA resins blended with DCPD or CL at a 50:50 mass ratio. Fig. 2(a) and (b) show the exothermic peaks corresponding to isothermal cure. These curing temperatures were selected on the basis of the onset temperature of exothermic peak determined from standard dynamic scans of NCA resin blends.

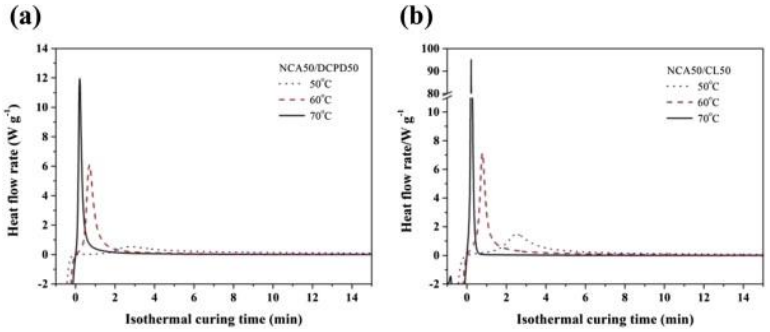

Fig. 2: Isothermal DSC thermogram of (a) NCA50/DCPD50 and (b) NCA50/CL50 at different curing temperatures.

Conversion, α, or degree of cure, is defined as:

$$\alpha = \frac{\Delta H_t}{\Delta H_{rxn}}$$

where ΔH_t is the heat generated up to time t during the cure reaction and ΔH_{rxn} is the total reaction heat per unit mass (J/g) from uncured ($\alpha = 0$) to fully cured ($\alpha = 1$). The conversion rate is defined as:

$$\frac{d\alpha}{dt} = \frac{dH/dt}{\Delta H_{rxn}}$$

where dH/dt represents the heat flow rate by DSC.

The NCA50-DCPD50 and NCA50-CL50 blends show the similar times for the maximum conversion rate to be reached. For both resin compositions, the time taken for maximum

conversion rate reduced significantly from about 2.5 min to about 12 s when the cure temperature was raised from 50 °C to 70 °C, exhibiting a significant influence of cure temperature on the ROMP cure kinetics. Compared to NCA/DCPD, the maximum conversion rate of NCA/CL resin is higher under the same curing condition, confirming a higher ROMP reactivity of CL than DCPD [21].

Fig. 3(a) and (b) show conversion with respect to time for both resins at different temperatures. The final conversion obtained after 1-h isothermal cure is shown in Table 1. At 70 °C, 90% of NCA/DCPD monomers were converted into the polymeric network in only 5 min, while NCA/CL reacted even faster. However, the fact that the conversion levels off below complete conversion means that a post-cure process, where the temperature is set above $T_{g\infty}$ (glass transition temperature in the fully cured state) is necessary to fully postcure the polymer network.

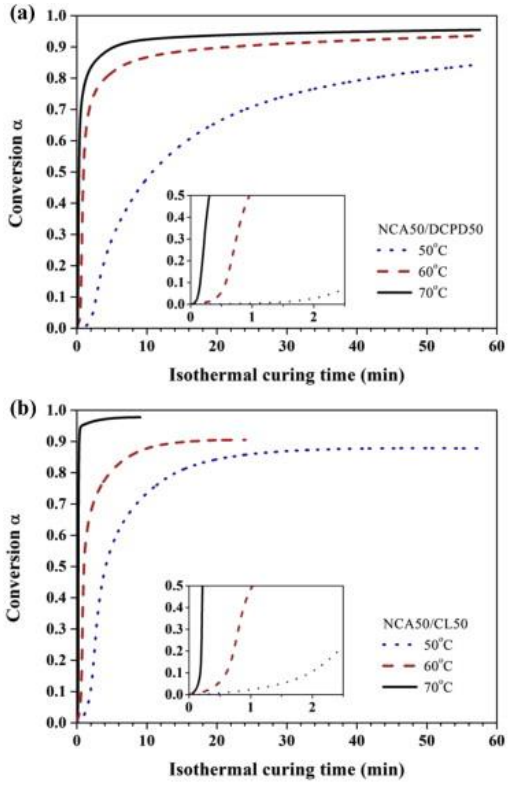

Fig. 3: Conversion as a function of time of (a) NCA50/DCPD50 and (b) NCA50/CL50 under isothermal cure at different curing temperatures.

Composition	Curing temperature (°C)	Time of (d*H*/d*t*) max (s)	(d*H*/d*t*) max (W/g)	Final conversion *α* (%)
NCA50/DCPD50	50	168 ± 2	0.53 ± 0.02	84.4 ± 1.4
	60	42.0 ± 0.6	6.1 ± 0.20	93.6 ± 1.2
	70	12.3 ± 0.3	12 ± 0.5	95.5 ± 1.2
NCA50/CL50	50	149 ± 1	1.5 ± 0.05	87.8 ± 1.1
	60	46.5 ± 0.3	7.1 ± 0.30	90.5 ± 1.5
	70	12.5 ± 0.4	95 ± 3.1	97.7 ± 1.2

Table 1: Selected isothermal cure data from Fig. 2 and Fig. 3.

Consequently, a cure schedule (described in Section 2.4) was proposed to fabricate bulk specimens for NCA resins with various levels of DCPD or CL loading. The curing temperature was set as 60 °C for all compositions as a trade-off cure condition for resins with higher comonomer loading (>30%) while ensuring high conversion rates for low comonomer loading (<30%). A post-cure temperature higher than $T_{g\infty}$ (135 °C) was selected to ensure full curing of resin without thermal degradation.

3.2. Glass transition temperature

Fig. 4 shows the evolution of glass transition temperature (T_g) as a function of cross-linking agent loading for the NCA/comonomer thermosets. The value of T_g here is determined by the maximum of dissipation factor peak from DMA measurements. It has been demonstrated that DSC is not sensitive to detect T_g accurately for NCA-dominant copolymers (NCA >80%), likely due to the effect of cross-linking and the multiple relaxation modes of fatty acid-based polymer chains [22].

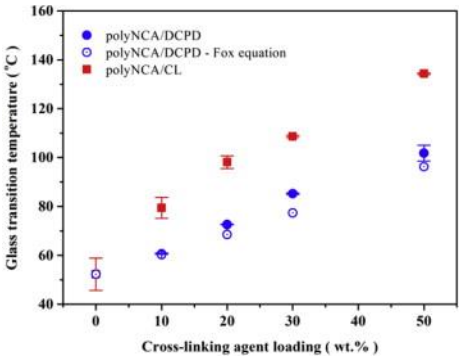

Fig. 4: Glass transition temperature (T_g) of polyNCA/DCPD and polyNCA/CL as a function of cross-linking agent loading.

In Fig. 4, polyNCA/DCPD and polyNCA/CL curves display a monotonic increase of T_g with the addition of cross-linking agents, with the value ranging from 52.3 °C for polyNCA to 101.8 °C and 134.3 °C for polyNCA/DCPD and polyNCA/CL, respectively, which is consistent with previous reports of copolymerization of linseed oil with DCPD or CL [11], [16] and [23]. In this study, the effect of DCPD and CL on the T_g shift behavior of the castor oil alcohol-based polymer is evaluated regarding the aforementioned two aspects: structural rigidity contribution and the crosslink density.

The Fox equation is a simple empirical model to predict the dependence of T_g on composition in a binary polymer system, usually polymer blends and copolymers. The T_g of neat polyNCA was measured as 52.3 °C and polyDCPD prepared by ROMP was reported as 153.9 °C previously [24]. Since the T_g of polyCL is not available yet for the difficulty of preparation, here only the T_g of polyNCA/DCPD is calculated as a function of its mass ratio based on the Fox equation.

$$\frac{1}{T_g} = \frac{w_1}{T_{g1}} + \frac{w_2}{T_{g2}}$$

T_{g1} and T_{g2} represent the glass transition temperatures of polyNCA and polyDCPD, respectively, while w_1 and w_2 are the corresponding mass fractions. A positive deviation of experimental T_g from Fox's prediction beyond error evaluation was observed for polyNCA/DCPD. The T_g increasing trend with DCPD loading differs from the linear relationship that was reported in previous NCO/NCA bio-polymer systems [8]. Nonetheless, it presented similarity to the T_g behavior of ROMP thermosets based on norbornene petroleum-derivatives with high cross-link density [25]. This observed deviation of T_g from the model could therefore be related to the high cross-linking density resulting from the high functionality of the NCA-comonomer compositions. Unlike Dilulin or NCO-based copolymers, of which the norbornenyl functionality per molecule is about 0.8–1, the NCA monomer affords a high cross-linked network by itself due to 1.8 ROMP-reactive norbornene rings per molecule (f = 1.8). As the cross-linking comonomer, CL has two norbornene rings of equal reactivity (f = 2), while DCPD (in terms of *endo* isomer) is able to lightly cross-link due to 20% of cyclopentene ring-opening except for norbornene ring-opening ($f \approx 1.2$) [26]. It is expected that a low-molecular-weight comonomer with high functionality, such as DCPD and CL, would tune the cross-link density of NCA around a high level. The altered T_g – composition dependence of polyNCA/DCPD from the model may reflect the reduction of free mobility of chain segments by the strong interaction in such a highly cross-linked system.

Besides, the higher T_g shown in polyNCA/CL compared to polyNCA/DCPD at the same comonomer loading is also associated with CL's higher functionality. CL retains a bicyclic structure after both norbornene groups undergoes ROMP and the structural units are theoretically all incorporated into copolymer backbone (in Scheme 1 (ii)). DCPD, on the other hand, is polymerized leaving with about 80% pendant cyclopentene rings, which gives lower contribution of rigid cyclic structure to the main polymer chains (in Scheme 1 (i)). As a result, CL appears to be a more efficient cross-linking agent than DCPD to improve T_g, as supported by the increasing difference of T_g between polyNCA/CL and polyNCA/DCPD with comonomer loading.

3.3. Thermo-mechanical properties

Fig. 5(a) and (b) shows the storage modulus and tan δ as a function of temperature for polyNCA/DCPD and polyNCA/CL samples. The E' of polyNCA/DCPD at 50% DCPD loading is 1514 ± 180 MPa at room temperature, an increase of 2.8 times that of neat polyNCA. Comparatively, E' of polyNCA/CL at 50% CL loading increased 2 times that of neat polyNCA, reaching up to 2046 ± 46 MPa. The significant modulus improvement in the glassy state results from the shift of the glass–rubber transition to higher temperatures. The nature of the sharp E' decrease, indicative of the glass transition, relative to cross-linking agent loading, differs considerably for polyNCA/DCPD and polyNCA/CL between. The E' decrease for polyNCA/DCPD appears to occur over a narrower temperature window and with a larger magnitude with increasing comonomer loading than that of polyNCA/CL. Interestingly for polyNCA/CL, further raising the CL loading from 30% towards 50%, the slope of the E' decrease reverts to the shape resembling the neat polyNCA.

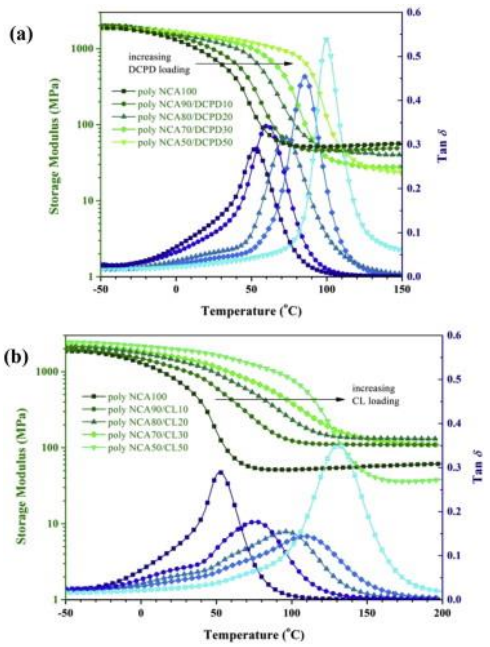

Fig. 5: Storage modulus and tan δ curves for (a) polyNCA/DCPD and (b) polyNCA/CL with increasing cross-linking agent loading.

Corresponding to the shift of E' decrease, the tan δ curve of polyNCA/DCPD in Fig 5(a) shows a single peak that becomes sharper and taller with increasing DCPD loading. A low-temperature and broad (between −20 °C and 40 °C) dissipation shoulder is present for both neat polyNCA and copolymers thereof, which decreases in intensity with the addition of DCPD. This shoulder indicates a broad, sub-glass transition in polyNCA, which was previously attributed to local crankshaft motions of ester groups between fatty chains and the conformational changes of the cyclopentane rings [27]. The diminishing intensity of sub-glass relaxation of polyNCA/DCPD results directly from the decrease in the NCA fraction. In Fig 6(a), the E'' of polyNCA/DCPD displays a similar decreasing dissipation shoulder with increasing DCPD loading. Meanwhile, the shoulder separates from the primary transition peak as T_g shifts to higher temperature.

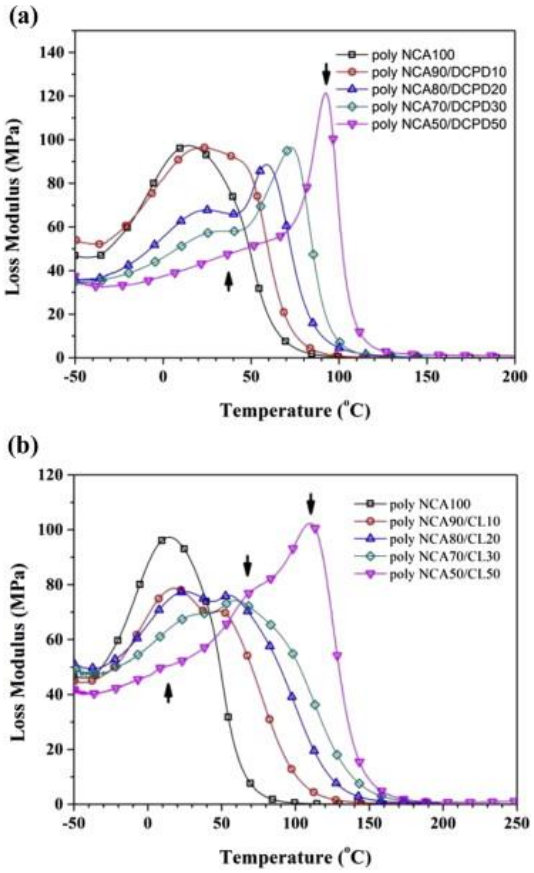

Fig. 6: Loss modulus curves of (a) polyNCA/DCPD and (b) polyNCA/CL with increasing cross-linking agent loading.

For polyNCA/CL, the tan δ curve shown in Fig. 5(b) develops with CL loading in a complicated manner. Compared to polyNCA/DCPD, the tan δ peak appears to span in broader temperature range and shrink in peak intensity by increasing CL loading up to 30%, which indicates the formation of a complex thermosetting network structure with high inhomogeneity. Three identifiable relaxation regions are observed in the tan δ peak with the highest 50% CL loading and assigned to low-, medium- and high-temperature region for convenience. The E'' curves plotted on a linear scale in Fig. 6(b) demonstrates these regions (pointed by black arrows) with better visibility. The E'' peak of the low-temperature relaxation region is stably located around 20 °C without changing with CL loading. With comparable results to the dissipation shoulder of polyNCA/DCPD, the low-temperature relaxation region of polyNCA/CL is also attributed to the sub-glass transition owing to NCA component. The medium- and high-temperature regions are expected be associated with the primary relaxations of multiple phases in the copolymer network, because the tan δ (or E'') peaks of both regions shift to higher temperature with the increase of CL loading. Last but not least, the decrease in intensity of the primary tan δ peak for polyNCA/CL discontinues at 30% CL loading while the peak remains shifting to higher temperatures. Further increase of CL loading up to 50% alters the evolving pattern of tan δ curves, which is consistent with the change in the glass-transitional E' decrease. In order to better explain the dynamic mechanical behavior of polyNCA/CL and polyNCA/DCPD, a correlation between cross-link density, T_g, and tan δ peak is established.

3.4. Evaluation of cross-link density

Fig. 5(a) and (b) show that in the rubbery plateau region, at temperatures above the glass transition, copolymers begin to show elastic characteristics. The crosslink density can be generally determined from the equilibrium shear modulus, which is commonly obtained at T_g + 50 °C in the rubbery plateau. The kinetic theory of rubber elasticity provides the following relationship [28]:

$$G = \frac{\Phi dRT}{M_c} \quad v_e = \frac{d}{M_c}$$

where Φ is the front factor, d is the density of the polymer, R is the gas constant, and T is the absolute temperature at T_g + 50 °C. M_c is the average molecular weight of elastically active network chains (EANCs) between cross-links, which is inversely proportional to the crosslink density v_e. The equation is only valid for lightly cross-linked rubbers that comply with the assumptions of Gaussian chains. Φ is assumed to be unity only when G < 10 MPa [29]. For highly cross-linked polymers, as is the case in this work, the EANC between two junctions are much shorter and less likely to be randomly curled. It was reported that Equation (5) does not give accurate predictions for highly cross-linked polymers such as epoxy and phenol-formaldehyde resins [30]. Hence, it has been suggested that when elastic shear modulus values exceed 10 MPa, showing a characteristic of non-Gaussian polymer chains, a modified empirical equation should be used to calculate cross-link density and is given as:

$$\log G = 6 + 23.6\frac{dM_x}{M_c}$$

where M_x is the molecular weight of the multifunctional cross-linked atoms plus the attached hydrogen atoms. The shear modulus can be substituted by the storage modulus, because for ideal rubber: $G = E'/3$. The density of polymers is unified for the sake of calculation. Cross-link density v_e and molecular weight between cross-links M_c of polyNCA/DCPD and polyNCA/CL are listed in Table 2. The calculated results are consistent with reasonable expectations: for example, M_c of neat polyNCA agrees with the molecular weight of NCA monomer unit ($C_{34}H_{52}O_4$, MW: 524.8).

	T_g (°C)				Cross-link density		
Copolymer composition	E'' peak	tan δ peak	tan δ peak max	E' at 30 °C (MPa)	v_e (mol/m^3)	M_c (g/mol)	Soluble fraction (%)
NCA100	13.4 ± 1.2	52.3 ± 6.6	0.31 ± 0.01	537 ± 86	2014	497	1.1
NCA90/DCPD10	21.9 ± 0.7	60.7 ± 0.2	0.34 ± 0.03	860 ± 45	1935	517	–
NCA80/DCPD20	58.6 ± 0.3	72.6 ± 0.1	0.32 ± 0.02	1120 ± 57	1875	533	–
NCA70/DCPD30	73.8 ± 1.1	85.2 ± 0.3	0.46 ± 0.01	1312 ± 75	1573	636	–
NCA50/DCPD50	92.9 ± 0.7	101.8 ± 3.2	0.53 ± 0.02	1455 ± 78	1454	689	0.9
NCA90/CL10	56.3 ± 7.9	79.4 ± 4.3	0.18 ± 0.01	1109 ± 58	2554	392	–
NCA80/CL20	56.4 ± 3.6	98.1 ± 2.6	0.15 ± 0.01	1340 ± 60	2689	372	–
NCA70/CL30	60.5 ± 1.8	108.6 ± 0.4	0.14 ± 0.01	1473 ± 33	2627	381	–
NCA50/CL50	113.0 ± 1.7	134.3 ± 0.3	0.35 ± 0.01	2046 ± 46	1759	569	1.0

Table 2: Dynamic mechanical properties and cross-link density determined by DMA.

As can be seen, the cross-link density decreases monotonically with the addition of DCPD, and the value of M_c increases from 497 g/mol to 689 g/mol. While this general trend is in agreement with the observed magnitude change in the relaxation peak in tan δ, it is noteworthy that T_g exhibits a non-linear increase with DCPD loading. The inverse relationship between T_g and cross-link density in polyNCA/DCPD system does not abide by the normal results from previous bio-thermoset studies. The decrease of cross-link density, due to the modification of multi-functionality between NCA and DCPD, is expected to have negative effect on T_g for the resulting thermosetting system. In fact, the T_g increase of polyNCA/DCPD appears to be dominantly influenced by increased structural rigidity rather than cross-linking effects. The main contributors, cyclopentane group and carbon–carbon double bond, which are characteristic in ROMP polymers based on norbornene-derivatives, endow chain segments with very low compliance and high activation energy for macroscopic cooperative movement. With increasing DCPD loadings, the thermoset network contained increased cyclic rigidity in lieu of the flexible backbone of the NCA fraction, resulting in an increase in T_g.

While investigating polyNCA/CL at a relatively low CL loading (<30 wt.%), a "typical" cross-linking effect for thermosets is observed. As the cross-link density increases, the tan δ peak representing the glass-to-rubber relaxation broadens, diminishes in intensity and shifts to higher temperature. The corresponding drop in E' also decreases in magnitude and expands over a wider temperature range. The increasing rate of v_e, however, slows down with the addition of CL and finally reaches a plateau between 20 wt.% and 30 wt.%. When the CL loading is further increased to 50 wt.%, v_e appears to decrease back to a value lower than polyNCA. The swelling percentage shown in Fig. 7 gives a qualitative interpretation of v_e which correlates well to the calculated v_e of polyNCA/CL. The impaired cross-linking effect by high CL loading is also manifested in the intensified E' decrease and tan δ relaxation peak indicating the transition of polyNCA/CL.

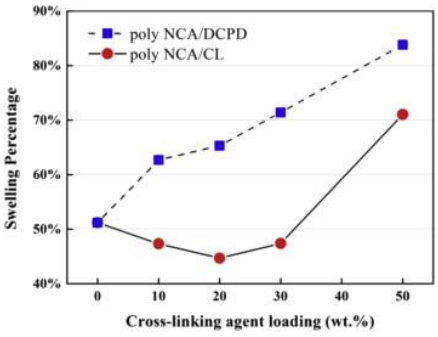

Fig. 7: Weight-based swelling percentage of polyNCA/DCPD and polyNCA/CL as a function of cross-linking agent loading.

Counterintuitive cross-linking trends have been observed previously with CL-copolymerized ROMP systems. In a Dilulin-CL copolymer, v_e leveled off at approximately 40 wt.% of CL loading [11]. In the case of a DCPD/CL copolymer, the effect of CL loading on v_e became negligible between 15 and 20 wt.% [31]. These phenomena could be related to reaction-induced microphase separation as a consequence of demixing on incipient formation of ROMP copolymer with high CL content [31]. At the initial curing stage, highly reactive CL is likely to

form individual cross-linked microgels before the formation of a cohesive network. After the reaction rate of CL significantly decreases as CL depletes, the propagation of NCA dominates the network growth till fully cured. This interpretation is evidenced by the multiple relaxations shown in the tan δ peak (Fig. 5(b)) and E'' peaks (Fig. 6(b)) of cured polyNCA/CL. In addition to the sub-T_g transition at around 10–40 °C, there are two primary transitions responsible for the multiple phases: the high T_g phase and the low T_g phase, according to the previous identification of the relaxation regions. The T_g of high T_g phase, determined by tan δ_{max} in the high-temperature region, increases substantially with CL loading. Hence, the high T_g phase is likely identified as CL-rich microgels. The T_g of low T_g phase is indicated by tan δ peak in the medium-temperature region and slowly shifts from 60 °C to 80 °C, which ascribes the low T_g phase to NCA-rich fraction. The generation of network heterogeneity, likely due to the differences in ROMP reactivity between NCA and CL, reduces the macroscopic cross-link density of the thermosets [32].

The soluble oligomer fraction determined by Soxhlet extraction was present in a few copolymer formulations, very low (around 1 wt.%, in Table 2), and independent of v_e for both polyNCA/DCPD and polyNCA/CL. This implies that cross-linking between NCA and the cross-linking agents is efficient and most monomer is incorporated into the polymer network.

3.5. Tensile properties

Fig. 8 illustrates the stress-strain behavior of polyNCA/DCPD and polyNCA/CL, determined by tensile testing. Two mass ratios (30/70 and 50/50) of each copolymer were compared to the neat polyNCA by investigating Young's modulus, maximum tensile strength, strain at break, and toughness (in Table 3). The two copolymers exhibited a different variation in tensile behavior with the addition of the cross-linking agents. Neat polyNCA exhibits ductile behavior with a yield point that occurs at about 2% strain, followed by plastic deformation and breaking at 12.4 ± 1.8% strain. As DCPD loading increases to 30% and 50%, a considerable improvement in Young's modulus, tensile strength, and toughness is observed for polyNCA/DCPD copolymers. PolyNCA50/DCPD50 reaches the highest tensile properties: Young's modulus of 1699 ± 428 GPa, tensile strength of 42.9 ± 0.6 MPa, toughness of 4.95 ± 0.55 J/m^3, and elongation at break (14.0 ± 1.6%). The improved tensile properties can be attributed to the effect of increasing T_g as well as declining cross-linking density by incorporating DCPD into polyNCA. Incorporation of a larger percentage of rigid cyclopentane rings into the backbone chains strengthens covalent and intermolecular bonding as well as the polymer's resistance upon stress, while the reduced cross-linking density is responsible for the larger elongation at break.

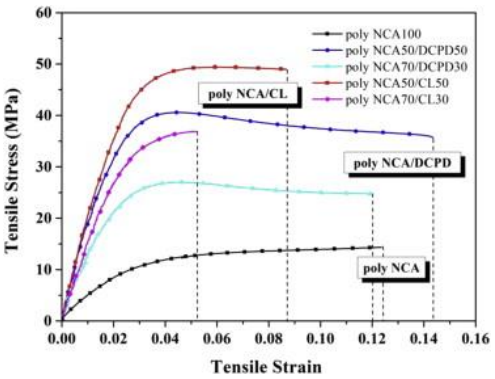

Fig. 8: Tensile stress-strain curves of polyNCA/DCPD and polyNCA/CL at various cross-linking agent loadings.

Composition	E (MPa)	σ_m (MPa)	ε_b (%)	Toughness (J/m^3)
NCA100	469 ± 47	15.5 ± 1.4	12.4 ± 1.8	1.37 ± 0.32
NCA70DCPD30	1213 ± 178	28.2 ± 0.5	11.6 ± 1.9	2.66 ± 0.43
NCA50DCPD50	1699 ± 428	42.9 ± 0.6	14.0 ± 1.6	4.95 ± 0.55
NCA70CL30	1639 ± 259	38.9 ± 0.2	5.2 ± 0.3	1.36 ± 0.10
NCA50CL50	2051 ± 128	52.2 ± 0.2	8.8 ± 0.8	3.59 ± 0.40

E = Young's modulus, σ_m = maximum tensile strength, ε_b = elongation at break.

Table 3: Tensile properties of polyNCA/DCPD and polyNCA/CL.

In comparison, polyNCA/CL copolymers exhibit lower strain at break in addition to increases in tensile strength and modulus when increasing CL loadings, demonstrating a trend to brittle failure. PolyNCA50/CL50 displays a slight increase in ε_b (by 3.6 ± 0.5) and toughness (by 2.23 ± 0.30 J/m^3) from polyNCA70/CL30, while E and σ_t continue to increase with CL loading. The shift of stress-strain curves according to CL loading is also influenced by the two variables of T_g and v_e but in a different way compared to polyNCA/DCPD system. The addition of CL increasing both T_g and cross-link density performs more efficient improvement on the tensile strength and modulus of polyNCA/CL, however detrimental to plastic deformation.

3.6. Thermal stabilities

Thermogravimetric analysis results for polyNCA/DCPD and polyNCA/CL are shown in Fig. 9(a) and (b). Assisted by the weight loss derivative, all TGA curves for the two groups of copolymers can be divided into three stages. The first stage represents a slow decline over the temperature range from 250 to 400 °C, which is probably related to the decomposition of side chains or branches that are lightly cross-linked within the thermosetting network. Soluble fractions or unreacted monomers may not be an influential factor to this stage because the Soxhlet extraction results evidenced that the resins were fully cured. The second stage ranging from 400 to 500 °C corresponds to a significant collapse in weight percentage. During this stage, the thermosets are subjected to fast decomposition of main chains in the network, the cleavage of

C=C bonds and ester groups for instance. The third stage, which extends to 650 °C, is responsible for the oxidation of residual char from the last stage.

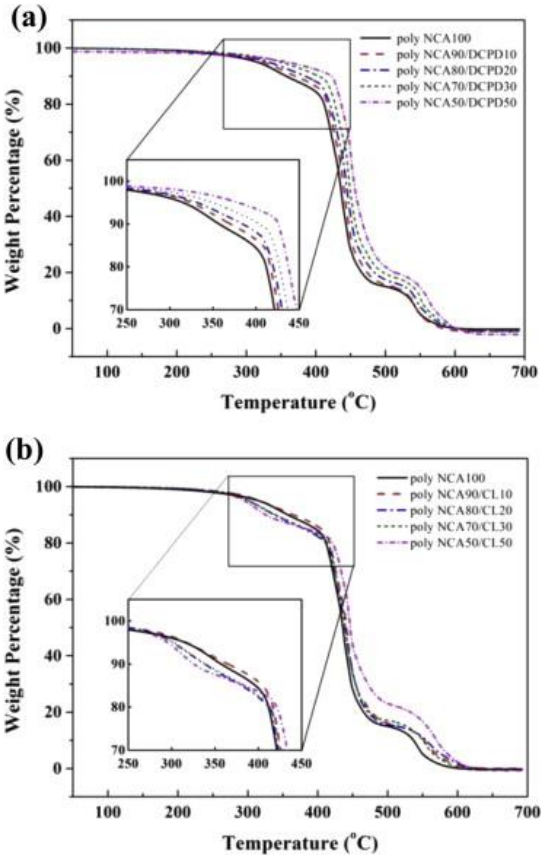

Fig. 9: Thermogravimetric analysis of (a) polyNCA/DCPD and (b) polyNCA/CL with increasing cross-linking agent loading.

As shown in Fig. 9(a), the weight loss curve is elevated stepwise for all three stages with the increase of DCPD loading in polyNCA/DCPD. The cross-linking of rigid cyclic moiety from DCPD imparts better thermal stability to the bio-based NCA polymer. Fig. 9(b) shows that polyNCA/CL does not exhibit such gradient shift with CL loading to polyNCA/DCPD. The weight loss of polyNCA/CL appear below neat polyNCA during the first degradation stage, as illustrated in the inset graph. The reason can be due to the formation of pronounced heterogeneity in the polyNCA/CL network. In a less homogeneous polyNCA/CL compared to polyNCA/DCPD, higher number of dangling chains that are loosely tied to the main network may be subjected to de-bonding and oxidization at early elevated temperature. PolyNCA/CL's resistance to degradation is therefore limited due to its network heterogeneity.

4. Conclusions

Norbornenyl-functionalized castor oil alcohol (NCA) was prepared and copolymerized with two cross-linking agents: DCPD and CL. CL exhibits higher ROMP reactivity than DCPD in curing with NCA. With increasing loading of cross-linking agents, the glass transition temperature,

storage modulus and tensile properties of both polyNCA/DCPD and polyNCA/CL increases significantly in a different manner, which is ascribed to the molecular structure and functionality of the cross-linking agents. The glass transition region of the thermosets, however, exhibits a complex dependence on the cross-linking agent loading. This is attributed to changes in cross-link density concomitant with the enhanced structural rigidity. These two factors also influence the ductile/brittle tensile behaviors of polyNCA/DCPD and polyNCA/CL. Structural heterogeneity causes the diminished thermal stability of polyNCA/CL compared to polyNCA/DCPD.

Acknowledgment

This material is based upon work supported by the National Science Foundation under Grant No. CMMI1348747. We are also thankful to Professor Richard Larock from the Department of Chemistry at Iowa State University (ISU) for the use of lab equipment for monomer preparation. Additionally, we thank Dr. David Grewell and Mr. Russell Huffman from the Department of Agricultural and Biosystems Engineering at ISU for their careful assistance in the preparation of tensile testing samples.

References

[1] G. Lligadas, J.C. Ronda, M. Galia, V. Cadiz. Mater Today, 16 (9) (2013), pp. 337–343

[2] S.N. Khot, J.J. Lascala, E. Can, S.S. Morye, G.I. Williams, G.R. Palmese, *et al.* J Appl Polym Sci, 82 (3) (2001), pp. 703–723.

[3] Y. Xia, R.C. Larock. Green Chem, 12 (11) (2010), p. 1893

[4] M.A.R. Meier, J.O. Metzger, U.S. Schubert. Chem Soc Rev, 36 (11) (2007), pp. 1788–1802

[5] R.P. Wool. 4-Polymers and composite resins from plant oils. R.P. Wool, X.S. Sun (Eds.), Bio-based polymers and composites, Academic Press, Burlington (2005), pp. 56–113

[6] E. Can, S. Kusefoglu, R.P. Wool. J Appl Polym Sci, 83 (5) (2002), pp. 972–980

[7] Y. Xia, Y.S. Lu, R.C. Larock. Polymer, 51 (1) (2010), pp. 53–61

[8] Y. Xia, R.C. Larock. Polymer, 51 (12) (2010), pp. 2508–2514

[9] W. Jeong, T.C. Mauldin, R.C. Larock, M.R. Kessler. Macromol Mater Eng, 294 (11) (2009), pp. 756–761

[10] P. Badrinarayanan, Y.S. Lu, R.C. Larock, M.R. Kessler. J Appl Polym Sci, 113 (2) (2009), pp. 1042–1049

[11] T.C. Mauldin, K. Haman, X. Sheng, P. Henna, R.C. Larock, M.R. Kessler. J Polym Sci Part A Polym Chem, 46 (20) (2008), pp. 6851–6860.

[12] P.P. Kundu, R.C. Larock. Biomacromolecules, 6 (2) (2005), pp. 797–806

[13] F.K. Li, J. Hasjim, R.C. Larock. J Appl Polym Sci, 90 (7) (2003), pp. 1830–1838

[14] P.R. Hondred, L. Salat, J. Mangler, M.R. Kessler. J Appl Polym Sci, 131 (12) (2014)

[15] J.X. Chen, M.D. Soucek, W.J. Simonsick, R.W. Celikay. Polymer, 43 (20) (2002), pp. 5379–5389

[16] P. Henna, R.C. Larock. J Appl Polym Sci, 112 (3) (2009), pp. 1788–1797

[17] P.H. Henna, M.R. Kessler, R.C. Larock. Macromol Mater Eng, 293 (12) (2008), pp. 979–990

[18] J.K. Stille, D.A. Frey. J Am Chem Soc, 81 (16) (1959), pp. 4273–4275

[19] S. Biswas, K.D. Belfield, R.K. Das, S. Ghosh, A.F. Hebard. Chem Mater, 21 (23) (2009), pp. 5644–5653

[20] A.S. Jones, J.D. Rule, J.S. Moore, S.R. White, N.R. Sottos. Chem Mater, 18 (5) (2006), pp. 1312–1317

[21] X. Sheng, J.K. Lee, M.R. Kessler. Polymer, 50 (5) (2009), pp. 1264–1269

[22] E. Can, R.P. Wool, S. Küsefoğlu. J Appl Polym Sci, 102 (3) (2006), pp. 2433–2447

[23] Y. Xia, P.H. Henna, R.C. Larock. Macromol Mater Eng, 294 (9) (2009), pp. 590–598

[24] W. Jeong, M.R. Kessler. Chem Mater, 20 (22) (2008), pp. 7060–7068

[25] X. Sheng, M.R. Kessler, J.K. Lee. J Therm Anal Calorim, 89 (2) (2007), pp. 459–464

[26] L. Matejka, C. Houtman, C.W. Macosko. J Appl Polym Sci, 30 (7) (1985), pp. 2787–2803

[27] S.A. Madbouly, Y. Xia, M.R. Kessler. Macromol Chem Phys, 214 (24) (2013), pp. 2891–2902

[28] G. Levita, S. Depetris, A. Marchetti, A. Lazzeri. J Mater Sci, 26 (9) (1991), pp. 2348–2352

[29] A.V. Tobolsky, M. Takahashi, R. Schaffha, D. Katz. J Polym Sci Part A General Pap, 2 (6pa) (1964), pp. 2749–2758.

[30] L.E. Nielsen. J Macromol Sci Rev Macromol Chem, C 3 (1) (1969), pp. 69–103

[31] Y.S. Yang, L.J. Lee. Polymer, 29 (10) (1988), pp. 1793–1800

[32] C.M. Sahagun, S.E. Morgan. Acs Appl Mater Interfaces, 4 (2) (2012), pp. 564–572